Compression-Induced Anomalous Subsidence in the Extensional Sedimentary Basin: A Numerical Study From the Pearl River Mouth Basin, Northern South China Sea Margin

Article *in* Geophysical Research Letters · September 2021

DOI: 10.1029/2021GL094750

CITATIONS
0

READS
156

8 authors, including:

Fucheng li
Chinese Academy of Sciences
17 PUBLICATIONS **170** CITATIONS
SEE PROFILE

Zhen Sun
Chinese Academy of Sciences
103 PUBLICATIONS **2,676** CITATIONS
SEE PROFILE

Weiwei Ding
Second Institute of Oceanography MNR
101 PUBLICATIONS **1,779** CITATIONS
SEE PROFILE

Hongfeng Yang
The Chinese University of Hong Kong
67 PUBLICATIONS **824** CITATIONS
SEE PROFILE

AGU ADVANCING EARTH AND SPACE SCIENCE

Geophysical Research Letters®

RESEARCH LETTER
10.1029/2021GL094750

Key Points:

- The central uplift accompanied by erosion or subsidence with abundant sediment accumulation may develop during the basin inversion
- Crustal thickness and tectonic quiescence are crucial factors determining whether the basin center will be uplifted or subsided
- Variation in the crustal thickness may be a mechanism for the different evolutionary pathways along the strike of the Pearl River Mouth Basin

Supporting Information:

Supporting Information may be found in the online version of this article.

Correspondence to:

F. Li and Z. Sun,
iamlifucheng@163.com;
zhensun@scsio.ac.cn

Citation:

Li, F., Sun, Z., Ding, W., Yang, H., Xie, H., Pang, X., et al. (2021). Compression-induced anomalous subsidence in the extensional sedimentary basin: A numerical study from the Pearl River Mouth Basin, northern South China Sea margin. *Geophysical Research Letters*, *48*, e2021GL094750. https://doi.org/10.1029/2021GL094750

Received 17 JUN 2021
Accepted 26 AUG 2021

Compression-Induced Anomalous Subsidence in the Extensional Sedimentary Basin: A Numerical Study From the Pearl River Mouth Basin, Northern South China Sea Margin

Fucheng Li[1,2], Zhen Sun[1,2], Weiwei Ding[3], Hongfeng Yang[4], Hui Xie[5], Xiong Pang[6], Hongbo Li[6], and Jinyun Zheng[6]

[1]Key Laboratory of Ocean and Marginal Sea Geology, South China Sea Institute of Oceanology, Innovation Academy of South China Sea Ecology and Environmental Engineering, Chinese Academy of Sciences, Guangzhou, China, [2]Southern Marine Science and Engineering Guangdong Laboratory (Guangzhou), Guangzhou, China, [3]Key Laboratory of Submarine Geosciences, State Oceanic Administration, Second Institute of Oceanography, Ministry of Natural Resources, Hangzhou, China, [4]Earth System Science Programme, Faculty of Science, The Chinese University of Hong Kong, Hong Kong, China, [5]Resources and Environment in Continental Shelf Sea and Deep Sea of Department of Education of Guangdong Province, Key Laboratory of Climate, Guangdong Ocean University, Zhanjiang, China, [6]China National Offshore Oil Corporation Ltd-Shenzhen/China National Offshore Oil Corporation Ltd-Deepwater, Shenzhen, China

Abstract Compressional uplift has long been considered as the basic response to basin inversion. However, significant discrepancies are recently observed in the Pearl River Mouth Basin (PRMB), where anomalous subsidence occurs during the Miocene compression phase. Whether the subsidence is another scenario that is associated with the tectonic inversion under certain circumstances remains unknown. Here we conduct systematic numerical modeling to explore the patterns of rift basin evolution from extension to compression. Our results show that two distinct inversion types develop depending on the stretching degree and tectonic quiescence. A less stretched continental crust would facilitate the uplift of basin center accompanied by erosion during shortening; otherwise, the basin center exhibits anomalous subsidence with abundant sediment accumulation. We further demonstrate that these two contrasting types, consistent with the Miocene evolutionary pathways of the eastern and western PRMB, respectively, are strongly conditioned by the along-strike variation of stretching degree during extension.

Plain Language Summary Uplift was previously considered as the only evolutionary pathway during basin inversion. Our expanded modeling study has demonstrated that the response is not unique. For example, the numerical results show that, when the continental crust is highly extended (e.g., to a thickness lower than 7 km) at the end of extension, the subsequent compression would promote the development of anomalous subsidence. By contrast, uplift and erosion of the basin center will occur only when the continental crust is slightly stretched. These results compare well with the along-strike variations observed in the Pearl River Mouth Basin (PRMB), northern South China Sea margin. The continental crust in the western PRMB has been stretched by a larger amount and thus is characterized by anomalously fast subsidence, whereas the eastern PRMB has undergone a smaller amount of crustal stretching and then is uplifted by several kilometers during the basin inversion.

1. Introduction

Extensional sedimentary basins may undergo transition from extensional to compressional regime due to a tectonic event which is often denominated as basin inversion (Cooper et al., 1989). Crustal thickening, erosional remnants, and reversely reactivated faults are commonly observed during basin inversion, for instance, in cases of the Alpine forelands (Ziegler, 1987) and Pyrenees (Ducoux et al., 2021; Garcia-Senz et al., 2000). Despite these general consensuses, there remain some exceptions as to the tectonic responses to the early stage inversion. Instead of causing compressional uplift, the inversion may also trigger a rapid subsidence that can accumulate abundant sediments, as occurred in the Pearl River Mouth Basin (PRMB).

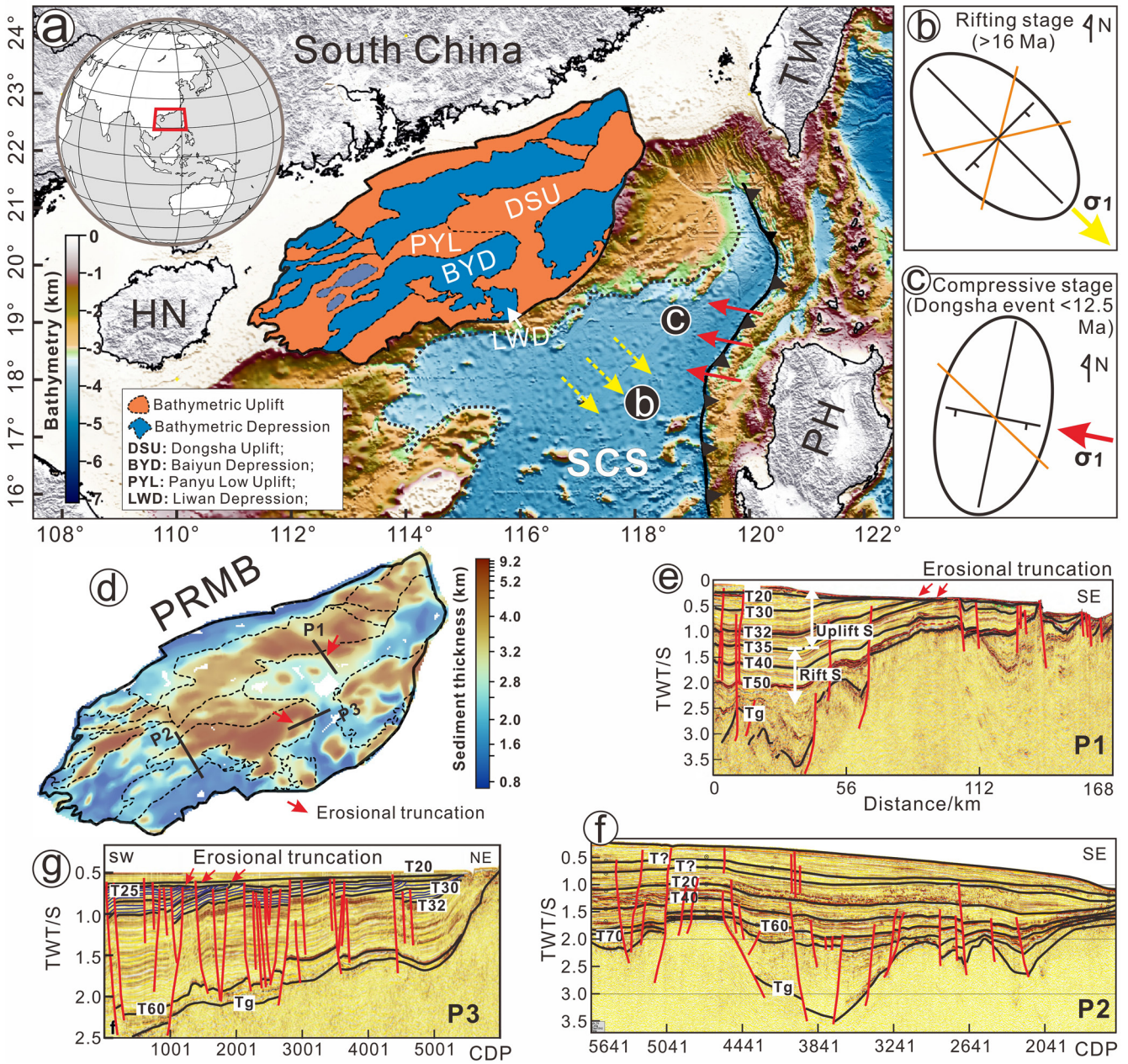

Figure 1. Tectonic setting of the Pearl River Mouth Basin (PRMB), northern South China Sea (SCS) margin. (a) Locations of the Depressions and Uplifts in the PRMB overlying the bathymetry map of the SCS. (b and c) The stress diagrams showing a SE stretching stress field in the PRMB at the rifting stage and a WNW compressive stress field during the compressional event (Franke et al., 2014; Hutchison, 2004; Sun et al., 2008, 2019). (d) Cenozoic strata thickness map of the PRMB. (e) Seismic profile across the eastern PRMB showing erosional truncation of the Middle Miocene strata (He et al., 2019). (f and g) Seismic profiles across the western PRMB showing a successive Miocene sedimentation process and a regional erosive process (Z. Xie et al., 2017), respectively.

The PRMB is a Cenozoic rift basin in the northern South China Sea (SCS) margin and undergoes compression only of several million years after it formed, so it well preserves evidences of the former and inverse patterns (Figure 1) (e.g., Barckhausen et al., 2014; Briais et al., 1993; Ding et al., 2020; F. Li et al., 2018; Sun et al., 2009, etc.). Previous studies have revealed that the PRMB exhibits different tectonic characteristics from east to west during the compression phase. In the eastern PRMB, multi-channel seismic profiles image a Miocene uplift event together with block faulting in the center, such as in the Dongsha (DS) Uplift (Gao et al., 2019; C. Li et al., 2015; Lüdmann & Wong, 1999; H. Xie et al., 2014; Z. Xie et al., 2017). For example, in profile P1, an erosional surface has been recognized truncating the Middle Miocene formation (T30, T32,

T35 in P 1, Figure 1e), and the Middle Miocene succession is gradually thinned and pinched out toward the DS Uplift. Many other geophysical studies also have revealed that the middle Miocene sediments in the DS Uplift are thin and, in places, even absent. Thereby, the DS Uplift is developed to be a relative sediment-poor region in the PRMB (Figure 1d).

By comparison with the east, the center of the western PRMB (e.g., the Panyu Low Uplift and Baiyun Sag/Depression) exhibits another scenario, where no significant Early to Middle Miocene erosional unconformity has been identified, except for few regional scales (Figures 1d and 1f). Instead, a rapid post-rift subsidence event with maximum rate up to 400 m/Myr can be widely observed in the west PRMB, where the excess subsidence caused by thermal contraction and is often called as "anomalous post-rift subsidence" (McKenzie, 1978; Wang et al., 2021; H. Xie et al., 2014; Zhao et al., 2011, etc.). Consequently, the Panyu Low Uplift and Baiyun Sag have evolved into the depocenters of the western PRMB with a complete sequence of Cenozoic sediments up to ∼10 km in thickness (Figure 1d). It should be noted that the western PRMB also has experienced compressional deformation during the Miocene epoch. For instance, besides the regional erosive surface (Figure 1f), the statistic of fault growth index in Baiyun Sag shows that many of the post-rift faults have experienced slight inversion and thus are compressive (Sun et al., 2014a, 2014b).

It has been widely believed that the Miocene uplift in the DS Uplift is related to a compressional event called the DS event/movement. This event refers to the convergence between Eurasia and the Philippine archipelago at 10.5–12.5 Ma (Figure 1c, P. Li & Rao, 1994; Pang et al., 2007; Sun et al., 2014a, 2014b; Wu et al., 2014). The stresses at the convergent plate boundaries transmit over distances up to ∼300 km into the PRMB, causing a continuous basement uplift accompanied by erosion. Although the collision-related compression appears to be widely distributed in the SCS area, its effects have long been considered to be limited to the eastern PRMB, largely because of the prevailing assumption that tectonic uplift/erosion is the only corresponding result of basin inversion. Indeed, the DS event is coeval with the anomalous Miocene subsidence in the Baiyun Sag, but whether there also exists a causal relationship between these two geological events is still unknown. Several hypotheses have attempted to interpret the anomalous subsidence as results of deep crustal flow (Dong et al., 2020; Liao et al., 2011), renewed thermal cooling (X. Xie et al., 2006), or reactivated extension (e.g., Clift & Lin, 2001). However, direct evidences for their existence are still lacking. The convergence-related compression by contrast can be conceived as a scientifically plausible and observationally supported mechanism. Thereby, it is necessary to evaluate whether the convergence-related compression can cause anomalous subsidence and, if so, under which condition does the compression contribute to the uplift or the anomalous subsidence?

Several numerical studies have been performed to investigate the process of basin inversion, but their models mainly focus on discussing the uplift patterns or orogenic evolutions that are determined by the interplay of many factors, such as thermal history (Buiter et al., 2009), lithospheric strength (Dai et al., 2014; Van Wijk & Cloetingh, 2002), surface erosion (Pysklywec, 2006; Simpson, 2006), rift maturity (Jourdon et al., 2019), and forearc uplift (Menant et al., 2020; Taylor et al., 2005). These factors are not the mechanisms to explain the DS event and contemporaneous anomalous subsidence occurred in the PRMB. Here we attempt to seek other deformation styles of inversion using a series of 2-D thermo-mechanical models. With these numerical models, we will also test the hypothesis that the stretching degree and tectonic quiescence duration are crucial in explaining the contrasting inversion types along the strike of the PRMB.

2. Numerical Model Description

Based on constraints from the case of the SCS, we use thermo-mechanical modeling to represent the process from extension to compression and further to discuss the deformation features during inversion. The geological evolutions of the SCS can be found in Text S1. A 2-D thermo-mechanical code modified after Gerya (2010) is applied in this study, which solves the incompressible creeping flows and heat transfer equations in the model domain. For more details about the governing equations and material parameters, please refer to Supporting Information S1 and the example of "viscoelastic-plastic extension" in the reference book of Gerya (2010).

Our initial model setup takes benefit of previous numerical studies that have successfully modeled the formation of a rift basin (e.g., Beaussier et al., 2019; Koptev et al., 2019; Liao & Gerya., 2017; Pérez-Gussinyé

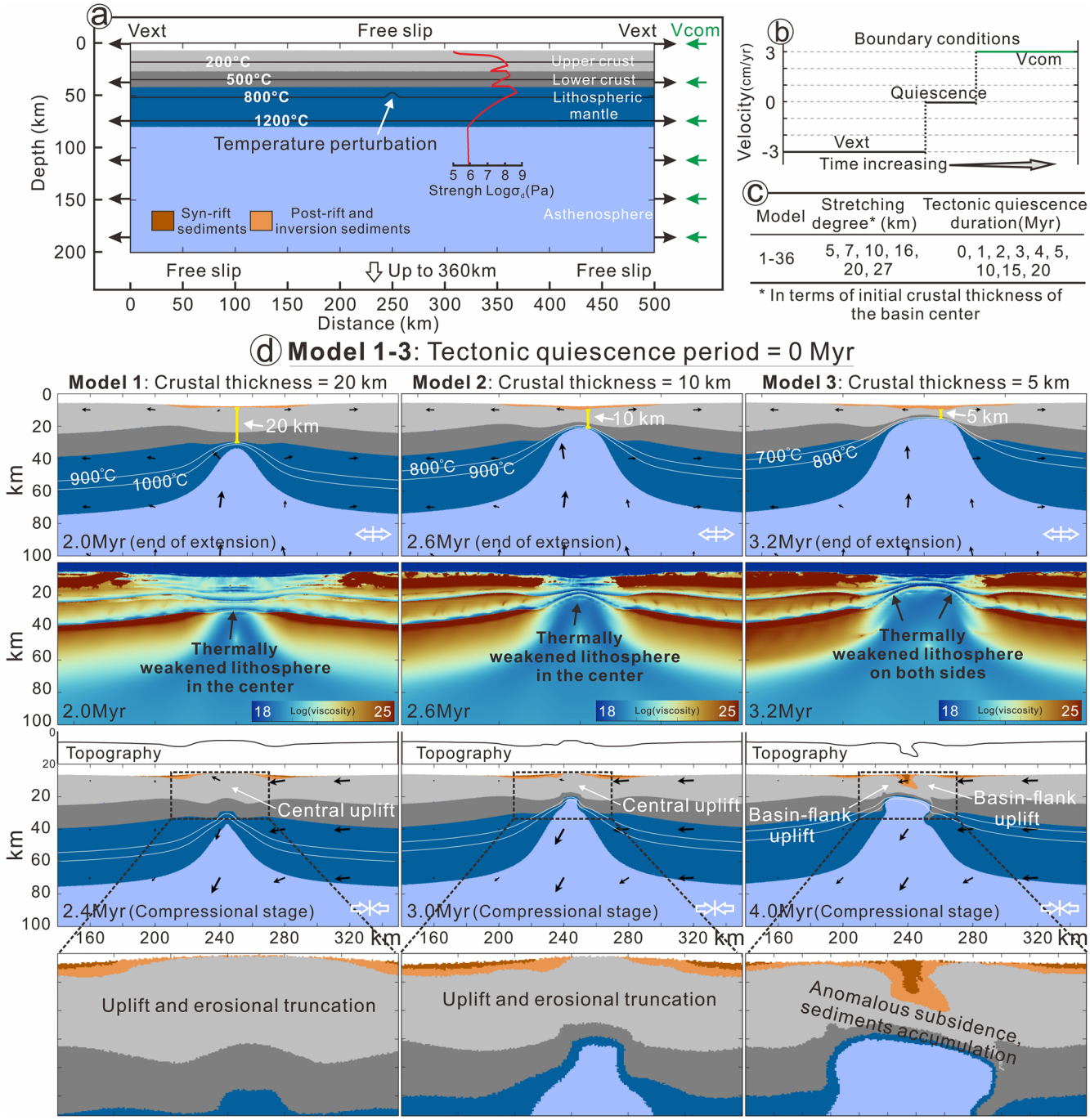

Figure 2. Initial model setup and evolution of reference model 1–3. (a) Enlarged 500 × 200 km domain of the initial 600 × 360 km model shown with composition, boundary conditions, initial temperature (black line), and yield strength profile (red line). (b) Time-varying velocity boundary conditions are applied on the left and right sides of the model domain. (c) Parametric studies testing the model sensitivities to the initial crustal thickness and tectonic quiescence duration. For more sensitivity tests for extension rates, please see Supporting Information S1. (d) Evolution of Set 1 with tectonic quiescence period of 0 Myr and initial crustal thickness of 20 km (model 1), 10 km (model 2), and 5 km (model 3) in the center. Viscosity fields at the end of the extension are illustrated in the diverging colormaps. The black arrows in represent velocities calculated for the given time step.

et al., 2006), especially in the SCS margin (Le Pourhiet et al., 2018; F. Li et al., 2019, 2020). The initial model consists of the upper crust, lower crust, lithospheric mantle, and asthenosphere of differing materials. The upper (20 km) and lower continental crust (15 km) are represented by quartzite and plagioclase rheology, respectively (Ranalli, 1995) (Figure 2a). The lithospheric mantle and asthenosphere are prescribed with dry

and wet olivine rheology (Ranalli, 1995). The material properties of all layers and the related references please see Table S1. A weak sticky layer with $\eta = 10^{18}$ Pa s, $\rho = 1{,}000$ kg/m^3 overlies the crust to provide a free-surface-like condition with C-condition of 0.08 (Crameri et al., 2012). The surface processes are calculated using simplified gross-scale erosion-sedimentation law (Burov & Cloetingh, 1997). We use a moderate sedimentation/erosion rate of 0.5 cm/yr within naturally observed ranges.

To achieve realistic modeling of basin inversion, we simulate three stages of the evolution cycle of a sedimentary basin: (a) basin formation, (b) tectonic quiescence (post-rift cooling), and (c) horizontal compression (Figure 2b). In the first stage, we assign a constant divergent velocity on the right-side boundary to model a mechanical extension of the continental lithosphere. The PRMB shows a highly variable crustal thickness ranging from ~21 to 23 km beneath the DS Uplift, to ~4–5 km beneath western BY Sag, which denotes that the basin may experience a different degree of lithospheric thinning along the strike. Thereby, we vary the extension duration from one model to another to reproduce the along-strike variations of crustal thickness (5, 7, 10, 16, 20, 27 km) (Figure 2c). Different extension rates are applied at the boundary to produce different initial crustal thicknesses, please see Supporting Information S1 for more sensitivity tests.

At the tectonic quiescence phase, we set the model velocity to zero to represent a window between the divergence and convergence phase. Quiescence durations of 0, 1, 2, 3, 4, 5, 10, 15, and 20 Myr are adopted in each model (Figure 2c). The compressional stage starts when a constant convergence velocity of 1.5 cm/yr is prescribed on the right side. Because we are interested in understanding the early response of the basin inversion, we have chosen not to include a long-term convergence history like the orogeny. Instead, the third stage continues for several million years which well preserve the structures of the former sedimentary basin and are able to compared with the present-day SCS. The velocity boundary condition on the bottom is permeable to satisfy an external free slip in the vertical direction.

The initial thermal structure of the continental lithosphere increases linearly from 0°C at the surface to 1380°C at the bottom of the lithospheric mantle (Figure 3c). A temperature gradient of 0.5°C/km is applied in the asthenospheric mantle. The left and right boundaries are thermally isolated. A small thermal heterogeneity (by elevating the 800°C isotherm by 4 km) is added in the lithospheric mantle, to initially generate a temperature perturbation in the middle of the model domain (Burg & Gerya, 2005; Hartz & Podladchikov, 2008).

3. Results

With several sets of numerical models, we investigate the effects of stretching degree and tectonic quiescence on the patterns of rift basin evolution during inversion. The models in each set consist of the same period of tectonic quiescence but different initial crustal thicknesses. We systematically vary the extension duration to obtain a different crustal thickness. The cases with final crustal thickness of 20, 10, and 5 km are selected for comparison (Figures 2d, 3, S1 and S2). The results of tectonic quiescence period of 10 and 15 Myr are shown in Supporting Information S1.

3.1. Set 1: Tectonic Quiescence Period of 0 Myr With Variable Crustal Thickness

The results in Figure 2d clearly show that, in addition to various crustal thickness, differences in the lithospheric thermal states can be observed among these models at the end of extension (*2 Myr in model 1, 2.6 Myr in model 2, 3.2 Myr in model 3*). In general, the less stretched model has a hotter lithosphere beneath the center, essentially because of the competitive effects of advection heating (caused by upwelling asthenospheric mantle) and diffusion cooling, or due to the different crustal heat production rates. For example, model **1** is stretched to 20 km and exhibits a maximum lithospheric temperature of ~900–1000°C beneath the center, while for a crustal thickness of 5 km (model **3**) approximately corresponds to the ~700–800°C isotherm (*2 Myr in model 1, 2.6 Myr in model 2, 3.2 Myr in model 3*).

As a direct result of increasing temperature, the viscosities of models are dramatically reduced. All the lithospheres in these models are thermally weakened with different degrees. For example, the viscosities of the lithosphere in models **1** and **2** were reduced to less than 10^{21} Pa s, and thus a large viscosity contrast can be observed between the center and the surrounding continental lithosphere (*2 Myr in model 1* and *2.6 Myr*

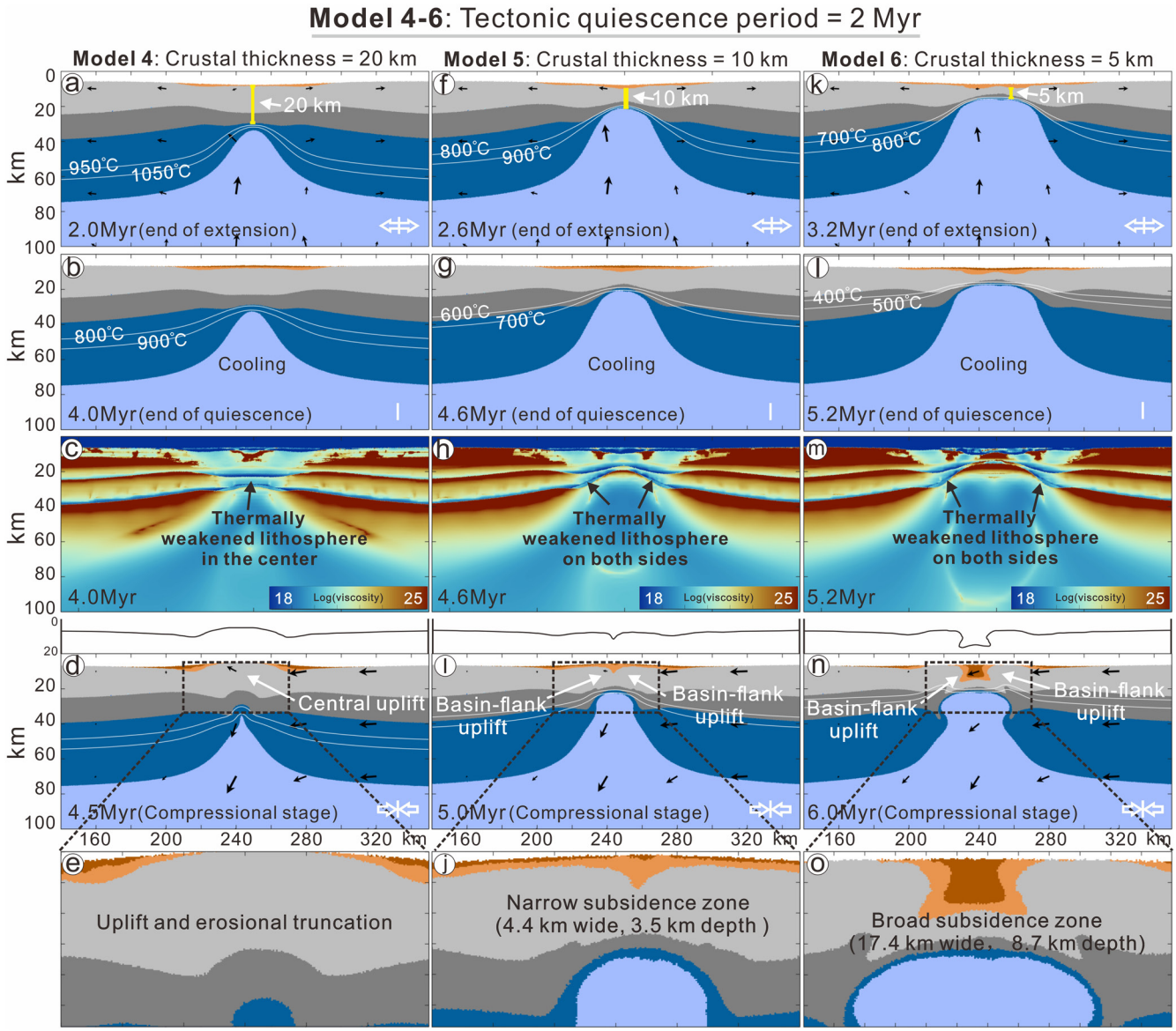

Figure 3. Evolution of Set 2 with tectonic quiescence period of 2 Myr and initial crustal thickness of 20 km (a, b, c, d, and e in model 4), 10 km (f, g, h, i, and j in model 5), and 5 km (k, l, m, n, and o in model 6) in the center. (c, h, m) Viscosity fields at the end of extension.

in model 2). By contrast, in model **3**, a region of high-strength mantle with a value up to 10^{23} Pa s still exists beneath the center at the end of the lithospheric extension (*3.2 Myr in model 3*). It is the difference in rheological behavior that eventually determine the patterns of rift basin evolution when the inversion starts.

The early stage compression is mainly accommodated by the deformation of the rheologically weak zone, and the different locations of weak zone further control the styles of inversion. For instance, uplifts in model **1** and model **2** develop in the basin center as the 20- and 10-km-thick crust is rheologically weak compared to the surroundings (*2.4 Myr in model 1* and *3 Myr in model 2*). Vertical thickening grows with continued shortening, and the uplifted syn-rift sediments are partially or completely removed by the erosional truncation, in agreement with findings from Buiter et al. (2009). Conversely, the deformation in model **3** is not focused on the center but is distributed on both sides of the basin (*4 Myr in model 3*). Observations of such situations are probably because a slice of strong lithospheric mantle exists beneath the center of model **3** (*3.2 Myr in model 3*), making the center not a preferred place to localize the initial compressive deformation. Continuous compression causes broad-scale folding of the basin-flank and, as a result, the center is

surrounded by high elevation ranges with peaks larger than several meters. Meanwhile, the basin center evolves into a subsiding syncline and thus accumulates thick successions over the pre-existing deposits (*4 Myr in model 3*).

3.2. Set 2: Tectonic Quiescence Period of 2 Myr With Variable Crustal Thickness

The second set, which has a quiescent period of 2 Myr (model **4**–**6**), also includes two different scenarios. However, compared to the first set, models with the same crustal thickness may result in distinct characteristics. For example, in contrast to set **1**, where the model thinned to 10 km is characterized by central uplift (model **2**), here the 10-km-thick crust causes flank uplift and central subsidence (model **5**). Such differences possibly stem from that a period of tectonic quiescence decreases the geothermal gradient due to conductive cooling or crustal heat production rates, for example, the maximum lithospheric temperature in model **5** cooling to ~600–700°C by 2 Myr (Figure 3g). This leads to thermal hardening of the lithosphere (Figure 3h) and further changes where the strain localization initially occurs, similar to those results reported by previous studies (e.g., Bassi et al., 1993; Sharples et al., 2015; Tetreault & Buiter, 2018).

The results also indicate that, even with the same style of inversion, differences can be observed between the models in set **1** and set **2,** for example, the size of the depression. For instance, model **6** has a depression approximately 17.4 km in width by 8.7 km in depth (Figure 3o), whereas the depression in model **3** is much smaller, 4.2 km in width by 10.1 km in depth (*4 Myr in model 3*, Figure 2d).

4. Discussion

4.1. Summary of Numerical Results

Two types of basin inversion may develop in the compression phase: (a) the central uplift accompanied by erosion and (b) central subsidence with abundant sediment accumulation. As shown in Figure 4a, we summarize the results in terms of inversion types as a function of the stretching degree (in terms of initial crustal thickness) and tectonic quiescence period. The results clearly show that both crustal thickness and tectonic quiescence are crucial factors determining whether the basin center will be uplifted or subsided during inversion.

Thinner crusts (≤7 km) demonstrate a tendency to cause subsidence in the center, whereas thicker crusts (≥16 km) are more likely to have central uplift. For other intermediate-thickness models (~8–15 km thick), the less the quiescence period is, the greater the likelihood of central uplift will occur. For example, the quiescent period should be less than 1 Ma to induce central uplift for a thickness of 10 km; otherwise, the center will subside at the stage of compression. As explained in the results, during extension, the crustal thickness determines the lithospheric strength through controlling the temperature field. A less degree of extension generally causes a higher temperature field in the center and thus facilitates the development of weaker lithosphere. When subject to horizontal compressional stress, the basin center is a preferred place for localization of the compressive deformation due to its lower strength with respect to the surrounding lithospheric domain and, as a consequence, the center evolves into a compressive uplift. In contrast, the highly stretched cases are characterized by relative high strength lithospheric mantle beneath the center. The subsequent shortening is accommodated by deformation on both sides of the strong lithospheric segment and thus causes a subsidence developed in the center. In summary, the patterns of rift basin evolution strongly depend on the mechanical strength of the lithosphere, which is controlled by the degree of lithospheric extension.

4.2. Comparison Between Models and Observations in the PRMB

The PRMB is a rift basin and contains a variable crustal thickness along its strike due to different degrees of lithospheric thinning. For example, at the end of the extension, the crustal thickness beneath the DS Uplift is predicted to be thicker than 21 km, whereas the Baiyun Sag indicates a minimum crustal thickness of ~4 km (Figures 4c and 4d). In the subsequent period of compression, the eastern and western PRMB exhibit distinctly different behaviors. The most obvious response in the east is the uplift of the DS Uplift, which eventually truncate the overlying rift structures and sedimentations, causing exposure of the pre-Cenozoic

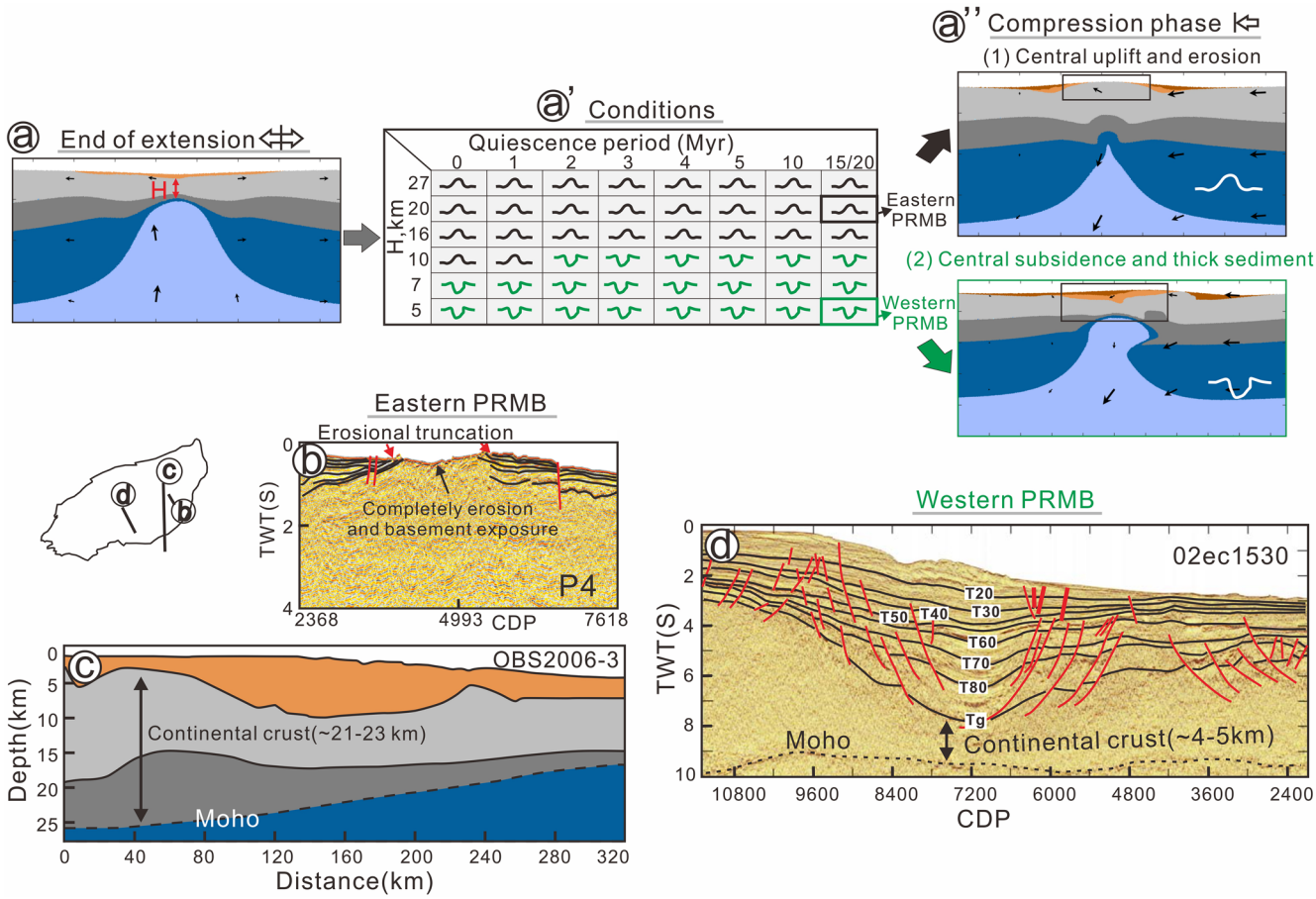

Figure 4. Phase diagram of the contrasting inversion types (a–a'') and comparison with the Pearl River Mouth Basin (PRMB) (b–d). (a) Lithospheric state at the end of extension. (a') Dependence of inversion types on the initial crustal thickness (*H*) and the tectonic quiescence period. (a'') Under different conditions, the models show types of (1) central uplift and (2) central subsidence during compressional phase. (b) Profile P4 across the eastern PRMB indicates uplift of the crystalline basement and partial/complete erosion of the overlying rift sediments. (c) Refraction seismic profile across the Dongsha Uplift shows characteristics of thick continental crust (~21–23 km) and basement uplift accompanied by sediment erosion (Wei et al., 2011). (d) Reflection profile across the BY Sag reveals that the west has a crustal thickness of ~4–5 km and is characterized by significant subsidence with abundant sediment accumulation.

basement (Lei et al., 2019; Lüdmann et al., 2001) (Figures 1e and 4b). By contrast, the west exhibits another scenario in which an anomalously fast subsidence event occurs in the center. For example, the sediment has a maximum thickness of ~6.48 s in the Baiyun Sag (Figure 4d), roughly corresponding with the converted depths between ~7.6 and ~8.2 km, which are rather close to the 8.0 km revealed by our models (Figure 4a''). These observations show similarities to our numerical models in which the styles of rift basin deformation largely depend on the crustal thickness (Figure 4a).

Therefore, our study demonstrates that variation in the crustal thickness may be a mechanism for the different evolutionary pathways along the strike of the PRMB. That is, the continental crust in the western PRMB has been stretched by a larger amount and thus is characterized by anomalously fast subsidence (Figure S2), whereas the eastern PRMB has undergone a smaller amount of crustal stretching and then is uplifted by several kilometers during the basin inversion (Figure 4a).

Although our results are well applicable to the PRMB, we note that the sedimentary architecture of the extensional basins may also be modulated by other factors such as lithospheric strength (Erdős et al., 2014; Huismans & Beaumont, 2011; Pérez-Gussinyé et al., 2020), plate motion (Duclaux et al., 2020), and heat advection (Karner & Gambôa, 2007; Yamato et al., 2013). In subduction zones, the interaction of deep mantle dynamics may also control the surface topography of continental upper plates in a form of continental tilting (Crameri & Lithgow-Bertelloni, 2018; Crameri et al., 2017). Their contributions are not evaluated in this

study. However, these factors affect the sediment morphologies by changing the final rift structures which have been simplified as amounts of stretching in our models. Despite simplifications, the extension models with different stretching degrees can be considered as end-member models of evolution of continental rifts. In addition, as we focus on the case of PRMB, the modes are meaningful to investigate the conditions of basin inversion in the SCS region.

5. Conclusions

We use 2-D thermo-mechanical models to investigate the evolution of PRMB from extension to compression and to understand the factors that determine the inversion types in general. Our models conclude that two types of basin inversion, (a) the central uplift accompanied by erosion and (b) central subsidence with abundant sediment accumulation, may develop depending on the stretching degree and the tectonic quiescence during the basin inversion. The two inversion types are developed along the strike of the PRMB as a consequence of the differences in the crustal stretching.

Data Availability Statement

Output data are available at https://doi.org/10.6084/m9.figshare.14340143.

Acknowledgments
This research was supported by the Guangdong NSF research team project (2017A030312002), Science and Technology Program of Guangzhou (202102020896), the Key Special Project for Introduced Talents Team of Southern Marine Science and Engineering Guangdong Laboratory (Guangzhou) (GML2019ZD0205), the K. C. Wong Education Foundation (GJTD2018-13), the Strategic Priority Research Program of the Chinese Academy of Science (XDA13010303), and the NSFC project (41606073). The China National Offshore Oil Corporation is much appreciated for providing the reflection seismic profiles. Figures were made using perceptually uniform diverging colormaps (Crameri et al., 2020).

References

Barckhausen, U., Engels, M., Franke, D., Ladage, S., & Pubellier, M. (2014). Evolution of the South China Sea: Revised ages for breakup and seafloor spreading. *Marine and Petroleum Geology*, *58*, 599–611. https://doi.org/10.1016/j.marpetgeo.2014.02.022

Bassi, G., Keen, C. E., & Potter, P. (1993). Contrasting styles of rifting: Models and examples from the eastern Canadian margin. *Tectonics*, *12*(3), 639–655. https://doi.org/10.1029/93tc00197

Beaussier, S. J., Gerya, T. V., & Burg, J.-P. (2019). Near-ridge initiation of intraoceanic subduction: Effects of inheritance in 3D numerical models of the Wilson Cycle. *Tectonophysics*, *763*, 1–13. https://doi.org/10.1016/j.tecto.2019.04.011

Briais, A., Patriat, P., & Tapponnier, P. (1993). Updated interpretation of magnetic anomalies and seafloor spreading stages in the South China Sea: Implications for the Tertiary tectonics of Southeast Asia. *Journal of Geophysical Research*, *98*(B4), 6299–6328. https://doi.org/10.1029/92jb02280

Buiter, S. J., Pfiffner, O. A., & Beaumont, C. (2009). Inversion of extensional sedimentary basins: A numerical evaluation of the localisation of shortening. *Earth and Planetary Science Letters*, *288*(3–4), 492–504. https://doi.org/10.1016/j.epsl.2009.10.011

Burg, J. P., & Gerya, T. (2005). The role of viscous heating in Barrovian metamorphism of collisional orogens: Thermomechanical models and application to the Lepontine Dome in the Central Alps. *Journal of Metamorphic Geology*, *23*(2), 75–95. https://doi.org/10.1111/j.1525-1314.2005.00563.x

Burov, E., & Cloetingh, S. (1997). Erosion and rift dynamics: New thermomechanical aspects of post-rift evolution of extensional basins. *Earth and Planetary Science Letters*, *150*(1–2), 7–26. https://doi.org/10.1016/s0012-821x(97)00069-1

Clift, P., & Lin, J. (2001). Preferential mantle lithospheric extension under the South China margin. *Marine and Petroleum Geology*, *18*(8), 929–945. https://doi.org/10.1016/s0264-8172(01)00037-x

Cooper, M. A., Williams, G. D., De Graciansky, P., Murphy, R., Needham, T., De Paor, D., et al. (1989). Inversion tectonics—A discussion. *Geological Society, London, Special Publications*, *44*(1), 335–347. https://doi.org/10.1144/gsl.sp.1989.044.01.18

Crameri, F., & Lithgow-Bertelloni, C. (2018). Abrupt upper-plate tilting during slab-transition-zone collision. *Tectonophysics*, *746*, 199–211. https://doi.org/10.1016/j.tecto.2017.09.013

Crameri, F., Lithgow-Bertelloni, C. R., & Tackley, P. J. (2017). The dynamical control of subduction parameters on surface topography. *Geochemistry, Geophysics, Geosystems*, *18*(4), 1661–1687. https://doi.org/10.1002/2017gc006821

Crameri, F., Schmeling, H., Golabek, G., Duretz, T., Orendt, R., Buiter, S., et al. (2012). A comparison of numerical surface topography calculations in geodynamic modelling: An evaluation of the 'sticky air'method. *Geophysical Journal International*, *189*(1), 38–54. https://doi.org/10.1111/j.1365-246x.2012.05388.x

Crameri, F., Shephard, G. E., & Heron, P. J. (2020). The misuse of colour in science communication. *Nature Communications*, *11*(1), 1–10. https://doi.org/10.1038/s41467-020-19160-7

Dai, L., Li, S., Lou, D., Liu, X., Suo, Y., & Yu, S. (2014). Numerical modeling of Late Miocene tectonic inversion in the Xihu Sag, East China Sea Shelf Basin, China. *Journal of Asian Earth Sciences*, *86*, 25–37. https://doi.org/10.1016/j.jseaes.2013.09.033

Ding, W., Sun, Z., Mohn, G., Nirrengarten, M., Tugend, J., Manatschal, G., & Li, J. (2020). Lateral evolution of the rift-to-drift transition in the South China Sea: Evidence from multi-channel seismic data and IODP Expeditions 367&368 drilling results. *Earth and Planetary Science Letters*, *531*, 115932. https://doi.org/10.1016/j.epsl.2019.115932

Dong, M., Zhang, J., Brune, S., Wu, S., Fang, G., & Yu, L. (2020). Quantifying postrift lower crustal flow in the northern margin of the South China Sea. *Journal of Geophysical Research: Solid Earth*, *125*(2), e2019JB018910. https://doi.org/10.1029/2019jb018910

Duclaux, G., Huismans, R. S., & May, D. A. (2020). Rotation, narrowing, and preferential reactivation of brittle structures during oblique rifting. *Earth and Planetary Science Letters*, *531*, 115952. https://doi.org/10.1016/j.epsl.2019.115952

Ducoux, M., Jolivet, L., Cagnard, F., & Baudin, T. (2021). Basement-cover decoupling during the inversion of a hyperextended basin: Insights from the Eastern Pyrenees. *Tectonics*, *40*(5). https://doi.org/10.1029/2020tc006512

Erdős, Z., Huismans, R. S., van der Beek, P., & Thieulot, C. (2014). Extensional inheritance and surface processes as controlling factors of mountain belt structure. *Journal of Geophysical Research: Solid Earth*, *119*(12), 9042–9061.

Franke, D., Savva, D., Pubellier, M., Steuer, S., Mouly, B., Auxietre, J. L., & Chamot-Rooke, N. (2014). The final rifting evolution in the South China Sea. *Marine and Petroleum Geology*, *58*, 704–720. https://doi.org/10.1016/j.marpetgeo.2013.11.020

Gao, J., Peng, X., Wu, S., Lüdmann, T., McIntosh, K., & Xu, Z. (2019). Different expressions of the crustal structure across the Dongsha Rise along the northeastern margin of the South China Sea. *Journal of Asian Earth Sciences*, *171*, 187–200. https://doi.org/10.1016/j.jseaes.2018.01.034

Garcia-Senz, J., Muñoz, J., & McClay, K. (2000). Inversion of Early Cretaceous extensional basins in the central Spanish Pyrenees. *American Association of Petroleum Geologists Bulletin*, *84*(9), 1428–1429. https://doi.org/10.1306/a96745bc-1738-11d7-8645000102c1865d

Gerya, T. (2010). *Introduction to numerical geodynamic modelling*. Cambridge University Press.

Hartz, H., & Podladchikov, Y. Y. (2008). Toasting the jelly sandwich: The effect of shear heating on lithospheric geotherms and strength. *Geology*, *36*(4), 331–334. https://doi.org/10.1130/g24424a.1

He, M., Zhu, W., Wu, Z., Zhong, G., Ren, J., & Liu, L. (2019). Neotectonic movement characteristics and hydrocarbon accumulation of the Pearl River Mouth basin. *China Offshore Oil and Gas*, *31*(5), 9–20.(in Chinese with English abstract).

Huismans, R., & Beaumont, C. (2011). Depth-dependent extension, two-stage breakup and cratonic underplating at rifted margins. *Nature*, *473*(7345), 74–78. https://doi.org/10.1038/nature09988

Hutchison, C. S. (2004). Marginal basin evolution: The southern South China Sea. *Marine and Petroleum Geology*, *21*(9), 1129–1148. https://doi.org/10.1016/j.marpetgeo.2004.07.002

Jourdon, A., Le Pourhiet, L., Mouthereau, F., & Masini, E. (2019). Role of rift maturity on the architecture and shortening distribution in mountain belts. *Earth and Planetary Science Letters*, *512*, 89–99. https://doi.org/10.1016/j.epsl.2019.01.057

Karner, G., & Gambôa, L. (2007). Timing and origin of the South Atlantic pre-salt sag basins and their capping evaporites. *Geological Society, London, Special Publications*, *285*(1), 15–35. https://doi.org/10.1144/sp285.2

Koptev, A., Beniest, A., Gerya, T., Ehlers, T. A., & Jolivet, L. (2019). Plume-induced breakup of a subducting plate: Microcontinent formation without cessation of the subduction process. *Geophysical Research Letters*, *46*. https://doi.org/10.1029/2018gl081295

Le Pourhiet, L., Chamot-Rooke, N., Delescluse, M., May, D. A., Watremez, L., & Pubellier, M. (2018). Continental break-up of the South China Sea stalled by far-field compression. *Nature Geoscience*, *11*, 605–609. https://doi.org/10.1038/s41561-018-0178-5

Lei, C., Ren, J., & Pang, X. (2019). Rift structures and its related unconformities on and adjacent the Dongsha Rise: Insights into the nature of the high-velocity layer in the northern South China Sea. *Marine Geophysical Research*. https://doi.org/10.1007/s11001-019-09381-x

Li, C. F., Li, J., Ding, W., Franke, D., Yao, Y., Shi, H., et al. (2015). Seismic stratigraphy of the central South China Sea basin and implications for neotectonics. *Journal of Geophysical Research: Solid Earth*, *120*(3), 1377–1399. https://doi.org/10.1002/2014jb011686

Li, F., Sun, Z., Pang, X., Liao, J., Yang, H., Xie, H., et al. (2019). Low-viscosity crustal layer controls the crustal architecture and thermal distribution at hyper-extended margins: Modeling insight and application to the northern South China Sea margin. *Geochemistry, Geophysics, Geosystems*, *20*, 3248–3267. https://doi.org/10.1029/2019gc008200

Li, F., Sun, Z., & Yang, H. (2018). Possible spatial distribution of the Mesozoic volcanic arc in the present-day South China Sea continental margin and its tectonic implications. *Journal of Geophysical Research: Solid Earth*, *123*, 6215–6235. https://doi.org/10.1029/2017jb014861

Li, F., Sun, Z., Yang, H., Lin, J., Stock, J. M., Zhao, Z., et al. (2020). Continental interior and edge breakup at convergent margins induced by subduction direction reversal: A numerical modeling study applied to the South China Sea margin. *Tectonics*, *39*, e2020TC006409. https://doi.org/10.1029/2020tc006409

Li, P., & Rao, C. (1994). Tectonic characteristics and evolution history of the Pearl River Mouth Basin. *Tectonophysics*, *235*(1–2), 13–25.

Liao, J., & Gerya, T. (2017). Partitioning of crustal shortening during continental collision: 2-D thermomechanical modeling. *Journal of Geophysical Research: Solid Earth*, *122*(1), 592–606. https://doi.org/10.1002/2016jb013398

Liao, J., Zhou, D., Zhao, Z., Zhang, Y., & Xu, Z. (2011). Numerical modeling of the anomalous post-rift subsidence in the Baiyun Sag, Pearl River Mouth Basin. *Science China Earth Sciences*, *54*(8), 1156–1167. https://doi.org/10.1007/s11430-011-4184-3

Lüdmann, T., & Wong, H. K. (1999). Neotectonic regime on the passive continental margin of the northern South China Sea. *Tectonophysics*, *311*(1–4), 113–138. https://doi.org/10.1016/s0040-1951(99)00155-9

Lüdmann, T., Wong, H. K., & Wang, P. (2001). Plio–Quaternary sedimentation processes and neotectonics of the northern continental margin of the South China Sea. *Marine Geology*, *172*(3–4), 331–358. https://doi.org/10.1016/s0025-3227(00)00129-8

McKenzie, D. (1978). Some remarks on the development of sedimentary basins. *Earth and Planetary Science Letters*, *40*, 25–32. https://doi.org/10.1016/0012-821x(78)90071-7

Menant, A., Angiboust, S., Gerya, T., Lacassin, R., Simoes, M., & Grandin, R. (2020). Transient stripping of subducting slabs controls periodic forearc uplift. *Nature Communications*, *11*(1), 1–10. https://doi.org/10.1038/s41467-020-15580-7

Pang, X., Chen, C., & Peng, D. (2007). *Deep-water fan system in the Pearl River Mouth Basin of South China Sea and its significant on petroleum*. Science Press. (In Chinese).

Pérez-Gussinyé, M., Andrés-Martínez, M., Araújo, M., Xin, Y., Armitage, J., & Morgan, J. (2020). Lithospheric strength and rift migration controls on synrift stratigraphy and breakup unconformities at rifted margins: Examples from numerical models, the Atlantic and South China Sea margins. *Tectonics*, *39*(12), e2020TC006255.

Pérez-Gussinyé, M., Morgan, J., Reston, T., Ranero, C. (2006). The rift to drift transition at non-volcanic margins: Insights from numerical modelling. *Earth and Planetary Science Letters*, *244*(1-2), 458–473. https://doi.org/10.1016/j.epsl.2006.01.059

Pysklywec, R. N. (2006). Surface erosion control on the evolution of the deep lithosphere. *Geology*, *34*(4), 225–228. https://doi.org/10.1130/g21963.1

Ranalli, G. (1995). *Rheology of the Earth* (2nd ed.). Chapman and Hall.

Sharples, W., Moresi, L. N., Jadamec, M. A., & Revote, J. (2015). Styles of rifting and fault spacing in numerical models of crustal extension. *Journal of Geophysical Research: Solid Earth*, *120*(6), 4379–4404. https://doi.org/10.1002/2014jb011813

Simpson, G. (2006). Modelling interactions between fold–thrust belt deformation, foreland flexure and surface mass transport. *Basin Research*, *18*(2), 125–143. https://doi.org/10.1111/j.1365-2117.2006.00287.x

Sun, Z., Lin, J., Qiu, N., Jian, Z., Wang, P., Pang, X., et al. (2019). The role of magmatism in the thinning and breakup of the South China Sea continental margin. *National science review*, *6*(5), 871–876. https://doi.org/10.1093/nsr/nwz116

Sun, Z., Xu, Z., Sun, L., Pang, X., Yan, C., Li, Y., et al. (2014). The mechanism of post-rift fault activities in Baiyun sag, Pearl River Mouth basin. *Journal of Asian Earth Sciences*, *89*, 76–87. https://doi.org/10.1016/j.jseaes.2014.02.018

Sun, Z., Zhong, Z., Keep, M., Zhou, D., Cai, D., Li, X., et al. (2009). 3D analogue modeling of the South China Sea: A discussion on breakup pattern. *Journal of Asian Earth Sciences*, *34*(4), 544–556. https://doi.org/10.1016/j.jseaes.2008.09.002

Sun, Z., Zhong, Z. H., Zhou, D., Pang, X., & Xu, H. (2008). Dynamics analysis of the Baiyun sag in the Pearl River Mouth Basin, north of the South China Sea. *Acta Geologica Sinica-English Edition*, *82*(1), 73–83.

Taylor, F. W., Mann, P., Bevis, M. G., Edwards, R. L., Cheng, H., Cutler, K. B., & Recy, J. (2005). Rapid forearc uplift and subsidence caused by impinging bathymetric features: Examples from the New Hebrides and Solomon arcs. *Tectonics*, *24*(6). https://doi.org/10.1029/2004tc001650

Tetreault, J. L., & Buiter, S. J. H. (2018). The influence of extension rate and crustal rheology on the evolution of passive margins from rifting to break-up. *Tectonophysics*, *746*, 155–172. https://doi.org/10.1016/j.tecto.2017.08.029

Van Wijk, J., & Cloetingh, S. (2002). Basin migration caused by slow lithospheric extension. *Earth and Planetary Science Letters*, *198*(3–4), 275–288. https://doi.org/10.1016/s0012-821x(02)00560-5

Wang, W., Dong, D., Wang, X., & Zhang, G. (2021). Three-stage tectonic subsidence and its implications for the evolution of conjugate margins of the southwest subbasin, South China Sea. *Journal of Oceanology and Limnology*, 1–17. https://doi.org/10.1007/s00343-020-0259-3

Wei, X. D., Ruan, A. G., Zhao, M. H., Qiu, X. L., Li, J. B., Zhu, J. J., & Ding, W. W. (2011). A wide-angle obs profile across the Dongsha uplift and Chaoshan depression in the mid-northern South China Sea. *Chinese Journal of Geophysics*, *54*(6), 1149–1160.

Wu, S., Gao, J., Zhao, S., Lüdmann, T., Chen, D., & Spence, G. (2014). Post-rift uplift and focused fluid flow in the passive margin of northern South China Sea. *Tectonophysics*, *615*, 27–39. https://doi.org/10.1016/j.tecto.2013.12.013

Xie, H., Zhou, D., Li, Y., Pang, X., Li, P., Chen, G., et al. (2014). Cenozoic tectonic subsidence in deepwater sags in the Pearl River Mouth Basin, northern South China Sea. *Tectonophysics*, *615*, 182–198. https://doi.org/10.1016/j.tecto.2014.01.010

Xie, X., Müller, R. D., Li, S., Gong, Z., & Steinberger, B. (2006). Origin of anomalous subsidence along the Northern South China Sea margin and its relationship to dynamic topography. *Marine and Petroleum Geology*, *23*(7), 745–765. https://doi.org/10.1016/j.marpetgeo.2006.03.004

Xie, Z., Sun, L., Pang, X., Zheng, J., & Sun, Z. (2017). Origin of the Dongsha event in the South China Sea. *Marine Geophysical Research*, *38*(4), 357–371. https://doi.org/10.1007/s11001-017-9321-8

Yamato, P., Husson, L., Becker, T. W., & Pedoja, K. (2013). Passive margins getting squeezed in the mantle convection vice. *Tectonics*, *32*(6), 1559–1570. https://doi.org/10.1002/2013tc003375

Zhao, Z.-X., Sun, Z., Xie, H., Yan, C.-Z., & Li, Y.-P. (2011). Cenozoic subsidence and lithospheric stretching deformation of the Baiyun deepwater area. *Chinese Journal of Geophysics*, *54*(6), 1161–1168. https://doi.org/10.1002/cjg2.1692

Ziegler, P. A. (1987). Compressional intra-plate deformations in the Alpine foreland—An introduction. *Tectonophysics*, *137*(1–4), 1–5. https://doi.org/10.1016/0040-1951(87)90223-x